Title

Human microglial cells as a therapeutic target in a neurodevelopmental disease model

Journal

Stem Cell Reports, 19(8)

ISSN

2213-6711

Authors

Mesci, Pinar

LaRock, Christopher N

Jeziorski, Jacob J

et al.

Publication Date

2024-08-01

DOI

10.1016/j.stemcr.2024.06.013

Peer reviewed

Stem Cell Reports
Article
ISSCR
OPEN ACCESS

Human microglial cells as a therapeutic target in a neurodevelopmental disease model

Pinar Mesci,[1,9,*] Christopher N. LaRock,[2,3] Jacob J. Jeziorski,[1] Hideyuki Nakashima,[7] Natalia Chermont,[1] Adriano Ferrasa,[4,5] Roberto H. Herai,[4,6] Tomoka Ozaki,[1] Aurian Saleh,[1] Cedric E. Snethlage,[1] Sandra Sanchez,[1] Gabriela Goldberg,[1] Cleber A. Trujillo,[1] Kinichi Nakashima,[7] Victor Nizet,[2] and Alysson R. Muotri[1,8,*]

[1]University of California, San Diego, School of Medicine, Department of Pediatrics/Rady Children's Hospital San Diego, Department of Cellular & Molecular Medicine, La Jolla, CA 92037, USA
[2]Department of Pediatrics, University of California San Diego School of Medicine and Skaggs School of Pharmacy and Pharmaceutical Sciences, La Jolla, CA 92037, USA
[3]Department of Microbiology and Immunology, Department of Medicine, Division of Infectious Diseases, Emory School of Medicine, Atlanta, GA 30322, USA
[4]Experimental Multiuser Laboratory (LEM), Graduate Program in Health Sciences (PPGCS), School of Medicine, Pontifícia Universidade Católica do Paraná (PUCPR), Curitiba, Paraná 80215-901, Brazil
[5]Department of Informatics (DEINFO), Universidade Estadual de Ponta Grossa (UEPG), Ponta Grossa, Paraná 84030-900, Brazil
[6]Research Department, Lico Kaesemodel Institute (ILK), Curitiba, Paraná, Brazil
[7]Department of Stem Cell Biology and Medicine, Graduate School of Medical Sciences, Kyushu University, Fukuoka, Japan
[8]University of California, San Diego, Kavli Institute for Brain and Mind, Center for Academic Research and Training in Anthropogeny (CARTA), La Jolla, CA 92093, USA
[9]Lead contact
*Correspondence: pmesci@gmail.com (P.M.), muotri@ucsd.edu (A.R.M.)
https://doi.org/10.1016/j.stemcr.2024.06.013

SUMMARY

Although microglia are macrophages of the central nervous system, their involvement is not limited to immune functions. The roles of microglia during development in humans remain poorly understood due to limited access to fetal tissue. To understand how microglia can impact human neurodevelopment, the *methyl-CpG binding protein 2* (*MECP2*) gene was knocked out in human microglia-like cells (MGLs). Disruption of the *MECP2* in MGLs led to transcriptional and functional perturbations, including impaired phagocytosis. The co-culture of healthy MGLs with MECP2-knockout (KO) neurons rescued synaptogenesis defects, suggesting a microglial role in synapse formation. A targeted drug screening identified ADH-503, a CD11b agonist, restored phagocytosis and synapse formation in spheroid-MGL co-cultures, significantly improved disease progression, and increased survival in MeCP2-null mice. These results unveil a MECP2-specific regulation of human microglial phagocytosis and identify a novel therapeutic treatment for MECP2-related conditions.

INTRODUCTION

Microglial cells originate from primitive hematopoiesis in the yolk sac during embryogenesis (Alliot et al., 1999; Ginhoux et al., 2010) and are the first glial cells appearing in the brain, coinciding with the beginning of synaptogenesis both in rodents and in humans (Kracht et al., 2020; Menassa and Gomez-Nicola, 2018; Reemst et al., 2016). Growing evidence supports that neuro-immune crosstalk is crucial for brain development and function (Cardona et al., 2006; Salter and Stevens, 2017). However, due to limited *in utero* access, little is known about the microglial contribution to healthy human brain development.

Here, we generated microglia-like cells (MGLs) from healthy human induced pluripotent stem cells (hiPSCs). By comparing the transcriptional profile of MGLs to human primary fetal microglia (FM), we noticed that many autism spectrum disorder (ASD)-related risk genes were expressed at similar levels between FM and MGL. Thus, we hypothesized that human microglia, besides playing a role in healthy neurodevelopment, could also be involved in conditions such as ASD, as previously suggested by *postmortem* analyses (Gandal et al., 2018; Parikshak et al., 2016).

We used induced pluripotent stem cell (iPSC) models to functionally evaluate the impact of a well-known ASD-risk gene *methyl-CpG binding protein 2* (*MECP2*) loss of function. We and others have previously shown that human and mouse neurons carrying mutant *MECP2* had decreased synaptogenesis, smaller soma size, reduced branching and neurite length, and altered neuronal network activity (Chao et al., 2007; Jiang et al., 2013; Kim et al., 2011; Marchetto et al., 2010; McGraw et al., 2011). While the role of *MECP2* in neurons is well documented, animal studies generated conflicting results regarding the contribution of *MECP2*-mutant microglial cells to brain development in male mice (Cronk et al., 2015; Derecki et al., 2012; Horiuchi et al., 2017; Jin et al., 2015; Maezawa and Jin, 2010; Schafer et al., 2016; Wang et al., 2015; Zhao et al., 2017).

Here, we revealed non-cell-autonomous roles of microglia in sculpting human synaptogenesis and neuronal connectivity and identified a therapeutic candidate. Our *in vitro* model will contribute to further determine the

impact of microglia on the developing human brain and help guide the discovery of new therapeutic alternatives for neurodevelopmental disorders.

RESULTS

Characterization of hiPSC-derived MGLs

We previously reported an efficient protocol to generate MGLs from iPSCs (Mesci et al., 2018) (Figure S1A), expressing classical microglial markers; CD68, CX3CR1, TREM2, IBA1, PU.1, CD11b, and P2YR12 (Figure S1B). Our MGLs closely recapitulated the transcriptomic signature of human primary FM at the level of both microglial transcriptional and homeostatic/activation factors (Figure S1C and Table S2). MGLs clustered closely with FM compared to iPSC-derived neurons and astrocytes (Figures S1D, S1E, and Table S2). MGLs highly expressed microglial genes, and at a lesser but similar fashion to FM, genes typically expressed by hematopoietic stem cells, primitive hematopoietic progenitor cells, erythro-myeloid precursors, but did not express the negatively associated genes such as *MS4A1*, *NCAM1*, *CD3G*, and *CD19* (Figure S1F and Table S2). As we hypothesized that microglial cells could play a role in neurodevelopment, we compared the expression of several ASD-related genes between MGL and FM. Out of 11 ASD-related genes displayed in Figure S1G, only PTEN, MEF2C, and TSC1 had statistically different expressions between MGL and FM, but the rest of the genes did not have a statistically different expression between MGL and FM. Therefore, we concluded that MGL and FM showed similar expression levels of ASD-related genes (Figure S1G, see Table S2 for the full list of ASD-related genes and their expression levels in MGL vs. FM).

The absence of MECP2 in MGLs leads to decreased cell viability and morphological and transcriptional changes

Given that MGL and FM revealed similar expression levels of ASD-related genes, we next wondered how MGLs could affect neurodevelopment. We chose to use a model of neuronal development perturbation by taking advantage of the similarities we observed between FM and MGL regarding the expression of several ASD-related genes. *MECP2* is an important gene for neural development, implicated in ASD and several other human conditions (Beyer et al., 2002; Chahrour et al., 2008; Cheung et al., 2011; Colantuoni et al., 2001; Guy et al., 2001; Kim et al., 2011; Lioy et al., 2011; Na et al., 2013; Schafer and Stevens, 2015; Sharma et al., 2019; Suter et al., 2014; Tillotson and Bird, 2020; Van den Veyver and Zoghbi, 2000; Ylisaukko-Oja et al., 2005). Still, the impact of *MECP2* mutations in human microglia during development remains debatable.

We selected patient-derived iPSC lines that lacked the MECP2 protein, denoted as knockout ("KO"), and generated isogenic CRISPR-corrected rescue lines by restoring the mutation, noted as "KO^R" (Figure S2A). We also included cell lines obtained from healthy donors (controls), indicated as "CTRL" (see Table S1). All cell lines have been previously characterized and published by our laboratory and others (Marchetto et al., 2010; Muotri et al., 2010; Nageshappa et al., 2016; Russo et al., 2018; Sharma et al., 2019; Trujillo et al., 2018; 2021; Zhang et al., 2016) (see experimental procedures). We confirmed by immunofluorescence that MGLs expressed MECP2 and then verified the loss of the protein in MGL KO lines and its re-expression on the KO^R MGLs (Figures 1A and S2B).

During MGL differentiation, we observed a period of significant latency in the generation of viable KO pre-MGL, occurring from day 24 to day 29 (Figure 1B), which later caught up with the CTRL and KO^R MGLs. This effect was linked to a lack of functional MECP2 since KO^R lines did not differ from CTRL MGLs in the generation of MGLs (Figure 1B). Pre-MGLs generated from CTRL, KO, and KO^R lines isolated from the media in suspension were then further differentiated into MGLs (Figures 1C and S2C), and their morphology was classified into three groups: round, elongated, or cell clumps (Figure 1D). In the absence of any external stimuli, both CTRL and KO^R MGLs generated approximately 60% elongated shaped cells, 35% round cells, and around 5% clumped cells (Figures 1E–1G), while KO MGLs generated about 50% of elongated shaped and 40% of round-shaped cells (Figures 1E–1G), suggesting the absence of MECP2 decreases the number of elongated cells. Also, KO MGLs exhibited a smaller surface area compared to CTRL or KO^R MGLs (Figure 1H). Alterations in morphology were attributable to the absence of MeCP2, as KO^R and CTRL MGLs surface areas were indistinguishable (Figures 1E–1H).

Next, we applied a targeted multiplex transcriptomic analysis using Human Myeloid Innate Immunity Panel gene expression array (NanoString Technologies), which includes 770 genes from 19 different pathways and processes (Butovsky et al., 2014) (Figures 1I, S2D, and Table S3). We confirmed that KO^R lines re-expressing the MECP2 protein clustered tightly with CTRL MGL lines, confirming observed gene expression changes were linked to the loss of MECP2 (Figures 1A and 1I). Compared to CTRL and KO^R MGL lines, 39 genes were differentially expressed in KO MGL lines (Figures 1I and S2D). We identified the top canonical pathways related to the CNS to be phagosome formation, integrin signaling, Fcγ

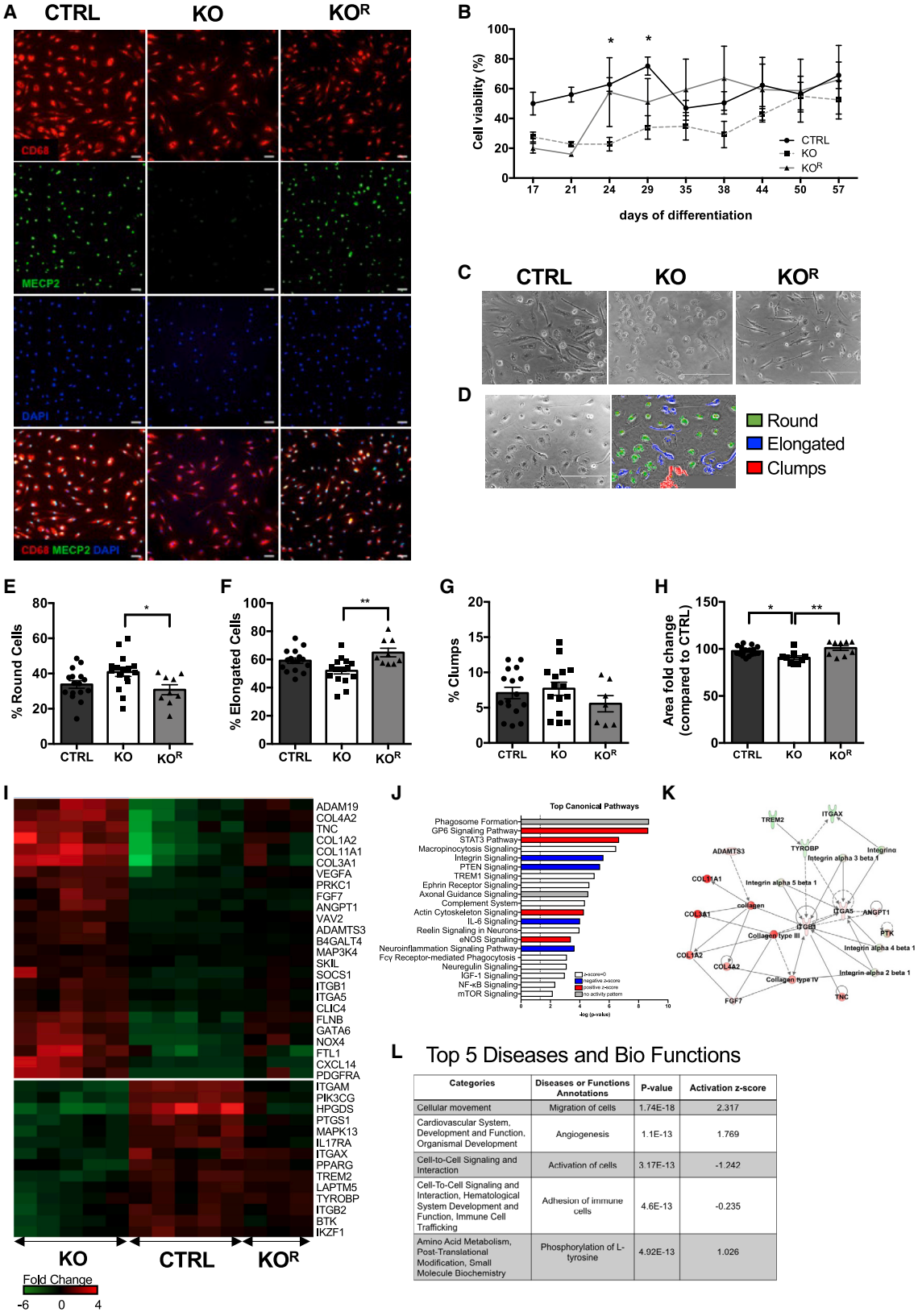

L Top 5 Diseases and Bio Functions

Categories	Diseases or Functions Annotations	P-value	Activation z-score
Cellular movement	Migration of cells	1.74E-18	2.317
Cardiovascular System, Development and Function, Organismal Development	Angiogenesis	1.1E-13	1.769
Cell-to-Cell Signaling and Interaction	Activation of cells	3.17E-13	-1.242
Cell-To-Cell Signaling and Interaction, Hematological System Development and Function, Immune Cell Trafficking	Adhesion of immune cells	4.6E-13	-0.235
Amino Acid Metabolism, Post-Translational Modification, Small Molecule Biochemistry	Phosphorylation of L-tyrosine	4.92E-13	1.026

(legend on next page)

receptor-mediated phagocytosis in macrophages and monocytes (Figure S2E), neuroinflammation (Figure S2F), axonal guidance, TREM1 signaling, complement system, and actin cytoskeleton signaling pathways (Figure 1J). The molecular network analyses showed reciprocal interactions between most dysregulated genes in KO MGLs, suggesting converging molecular pathways (Figures 1J–1L), including cell movement, cell-to-cell signaling, and cell adhesion (Figure 1L).

To detect additional pathway alterations caused by MECP2 loss beyond targeted myeloid genes and function transcriptomics, we further performed unbiased high-throughput messenger RNA sequencing (RNA-seq) on CTRL, KO^R, and KO MGLs (Figures S2G–S2K, and Table S3). These global transcriptome analyses revealed 2,513 differentially expressed genes with a p value <0.05 and a fold change greater than 1.25 (Figure S2J). Four genes were identified in common between the two transcriptomic analyses: *COL1A2*, *ITGAX*, *PTGS1*, and *TNC*. *COL1A2* and *TNC* were upregulated in targeted and untargeted transcriptome analyses, as well as shared canonical pathways, such as integrin signaling, actin cytoskeleton signaling, phagosome formation, and Fcγ receptor-mediated phagocytosis in macrophages and monocytes (Figures 1I, 1J, and S2I). Several other gene families belonging to the complement system, cathepsins, chemokine signaling, SIGLECs, and ER-phagosome formation were also found to be dysregulated between KO and CTRL/KO^R MGLs (Figure S2K). Collectively, our transcriptomic analyses provided converging evidence that the loss of MECP2 alters phagocytosis pathways.

MECP2 chromatin immunoprecipitation sequencing and proteomic assays on MGL

To assess whether MECP2 could directly regulate microglial function by occupying target genes or their promoters, we performed a MECP2 chromatin immunoprecipitation sequencing assay (MECP2 ChIP-seq) on KO^R and CTRL MGLs (Figures 2A–2G, S3A–S3C, and Table S4). As a negative control, we used KO MGLs and were unable to generate sequencing libraries due to the absence of MECP2 protein and/or binding. We found over 120,000 MECP2 occupation sites genome-wide on both KO^R and CTRL MGL samples, as previously observed by others (Rube et al., 2016; Skene et al., 2010). Focusing on common MECP2 occupation sites between KO^R and CTRL MGL samples (Figure 2B), 58,521 sites were identified, the majority located in introns and intergenic regions (Figures 2C, and Table S4). We hypothesized that sites on promoter regions would predict potential MECP2 downstream targets that regulate microglial functions. Such promoter-transcription starting site (TSS) regions represent 4,069 (6.95%) of the total MECP2 sites found in both MGL samples (Figure 2C). Among these, seven genes were shared in common with the targeted transcriptomics (*FLNB*, *ITGAM*, *LAPTM5*, *PDGFRA*, *PIK3CG*, *PPARG*, and *PTGS1*), and 653 genes overlapped with our untargeted RNA-seq (Table S4). Top canonical pathways obtained from genes in which MECP2 protein occupied

Figure 1. The absence of MECP2 leads to decreased cell viability and dysregulations in cell migration, integrin, and phagosome formation pathways in MGLs

(A) Representative images of CTRL, KO, and KO^R MGLs stained with CD68 and MeCP2 antibodies. Scale bar 10 μm.

(B) The percentage of cell viability was compared between different cell lines. Each data point shows the mean ± SEM, as indicated. Significance was tested using a two-way ANOVA with the Tukey's multiple comparison test (*p = 0.0304 and *p = 0.0247 for day 24 and 29, respectively) (three lines for CTRL MGLs and KO and two isogenic rescue lines for KO^R MGLs, n = 3 independent experiments for each sample at each time point).

(C) Bright-field images of CTRL, KO, and KO^R MGLs at day 7 of differentiation, scale bar 200 μm.

(D) Bright-field images of CTRL MGLs with (right) or without (left) masks that marked round (in green), elongated (in blue), or cell clumps (in red), scale bar 200 μm.

(E–H) Percentage of round cells, elongated cells, and cell clumps, respectively. (H) Area fold change compared to the control of CTRL, KO, and KO^R. One-way ANOVA with the Tukey's multiple comparison test was performed (*p = 0.0323, **p = 0.0022, and n.s. for E to G, respectively, for *p = 0.0149 and **p = 0.0021 for H (Each bar shows the mean ± SEM, each dot represents one sample, two different isogenic pairs, two different clones for CTRL with three independent experiments per sample).

(I) Heatmap showing the 39 differentially expressed genes (greater than 1.25-fold) between these two groups (KO n = 5 from two independent cell lines, two to three biological replicates, CTRL n = 5 from two independent cell lines, two to three biological replicates and KO^R n = 3 from two independent cell lines, one to two independent experiments $p < 0.05$, data were analyzed for statistical significance using Rosalind onramp software, see supplemental information, methods' section). Increasing fold changes compared to CTRL are marked in red while decreasing ones are in blue.

(J) Top canonical pathways were obtained with 39 differentially expressed genes (DEGs) using Ingenuity Pathway Analysis (IPA), where significance was calculated by the right-tailed Fisher's exact test ($p < 0.05$).

(K) The top network involving the majority of DEG obtained through IPA, genes that are downregulated are in green and upregulated are in red.

(L) Top 5 diseases and biological functions were obtained with IPA.

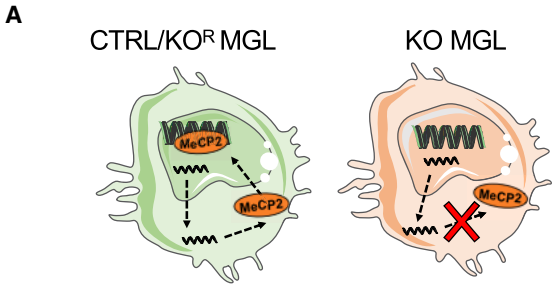

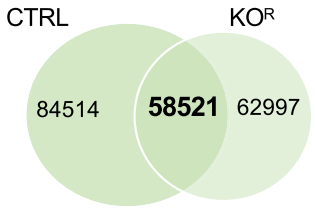

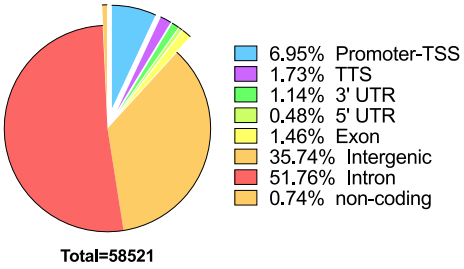

E

Gene name	Chromosome	Annotation	Distance
PPARG	3	promoter-TSS (NM_015869)	-639
LAPTM5	1	promoter-TSS (NM_006762)	-792
P2RY12	3	promoter-TSS (NM_022788)	-715
OLFML3	1	promoter-TSS (NM_020190)	-158
CYBB	X	promoter-TSS (NM_000397)	1
CXCL3	4	promoter-TSS (NM_002090)	-676
CCR5	3	promoter-TSS (NM_000579)	-126
CXCR2	2	promoter-TSS (NM_001557)	-4
CCR3	3	promoter-TSS (NM_178329)	-346
CCL13	17	promoter-TSS (NM_005408)	-629
CD93	20	promoter-TSS (NM_012072)	-158
C1QA	1	promoter-TSS (NM_001347465)	-247
C1QB	1	promoter-TSS (NM_000491)	-2
C1QTNF5	11	promoter-TSS (NM_001278431)	-256
C1QTNF6	22	promoter-TSS (NM_182486)	-268
C2	6	promoter-TSS (NM_001145903)	96
C3	19	promoter-TSS (NM_000064)	-91
C9	5	promoter-TSS (NM_001737)	-289
SIGLEC5	19	promoter-TSS (NM_003830)	-420
SIGLEC7	19	promoter-TSS (NM_001277201)	-341
SIGLEC14	19	promoter-TSS (NM_001098612)	-524
AXL	19	promoter-TSS (NM_001699)	-289
ITGAM	16	promoter-TSS (NM_000632)	-665
ITGA4	2	promoter-TSS (NM_001316312)	-663
MRC1	10	promoter-TSS (NM_002438)	-937

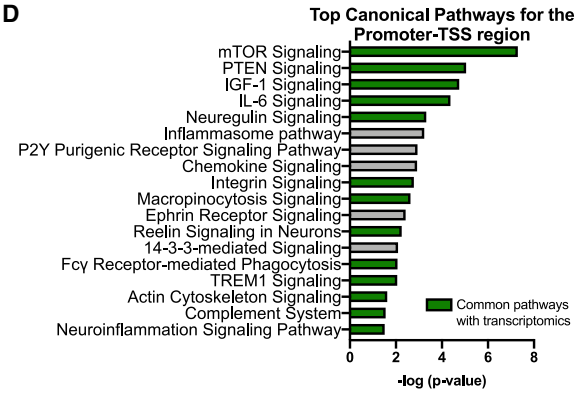

F

Top 5 known motifs

P-value	% of targets	% of background	Best Match
1e-371	2.09	0.49	CTCF (Zf)
1e-213	2.39	0.92	BORIS(Zf)
1e-212	6.46	3.76	PU.1(ETS)
1e-180	4.94	2.12	SpiB(ETS)
1e-164	9.29	6.33	ELF5(ETS)

G

Top 5 *de novo* motifs

P-value	% of targets	% of background	Best Match
1e-312	8.39	4.73	SpiB(ETS)
1e-272	1.54	0.36	BORIS(Zf)
1e-105	0.15	0.01	STAT5(Stat)
1e-81	3.70	2.39	PB0057.1Rxra_1
1e-77	9.66	7.54	FOS::JUN

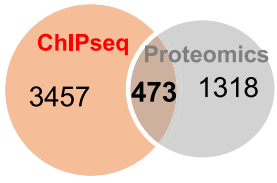

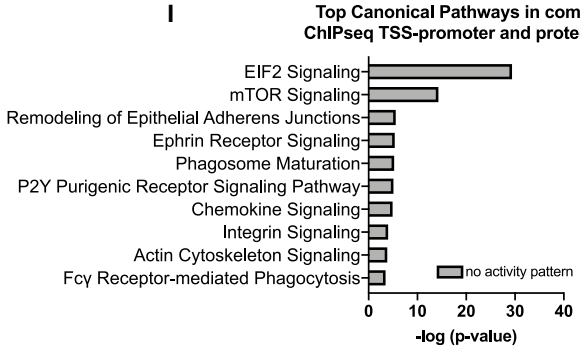

(legend on next page)

promoter regions included several previously revealed pathways from transcriptomics, including integrin signaling, Fcγ receptor-mediated phagocytosis in macrophages and monocytes, TREM1 signaling, complement system, neuroinflammation signaling pathway, and actin cytoskeleton signaling (Figure 2D). From the catalog of promoter-TSS occupation sites, MECP2 occupied the promoter region of two microglial marker genes (*P2RY12* and *OLFML3*), several chemokines, and their receptors (*CXCL3*, *CCR5*, *CXCR2*, *CCR3*, and *CCL13*), and *CYBB*—a gene involved in the generation of reactive oxygen species (ROS). MECP2 also occupied the promoter region of genes that belong to the complement system (*CD93*, *C1QA*, *C1QB*. *C1QTNF5*, *C1QTNF6*, *C2*, *C3*, and *C9*) and to the immunoregulatory receptors related to microglial engulfment (*SIGLEC5*, *SIGLEC7*, and *SIGLEC14*). Finally, MECP2 occupied the promoter of genes involved in the phagocytosis process (*AXL*, *ITGAM*, *ITGA4*, and *MRC1*) (Figure 2E). We found several known "binding" motifs: CTCF (Barski et al., 2007) (Homer), BORIS (Zf) (GSE32465, Homer), PU.1 (ETS) (GSE21512, Homer), SpiB (ETS) (GSE56857, Homer), and ELF5 (ETS) (GSE30407, Homer), but also discovered *de novo* motifs: SpiB (ETS) (GSE56857, Homer), BORIS (Zf) (GSE32465, Homer), STAT5 (Stat) (GSE12346, Homer), PB0057.1Rxa_1 (Jaspar), and FOS::Jun (Jaspar) (Figures 2F and 2G).

As a final tool to complete our search for microglial cell pathways altered upon loss of MECP2, we conducted a label-free liquid chromatography-mass spectrometry (LC-MS) proteomic analysis on CTRL, KO, and KO^{R} MGLs (Figures 2H, 2I, S3D–S3G, and Table S4), once again picking up pathways shared in common with targeted or bulk transcriptomics and as MECP2 ChIP-seq (Figure S3D). There were 473 targets revealed by proteomics in which MECP2 was found to occupy their promoter, pointing to canonical pathways, including phagosome formation, integrin signaling, phagosome maturation, and actin cytoskeleton signaling pathways (Figures 2H, 2I, and S3D–S3G). We noted several top causal networks having significant *Z* score alterations (activated or inhibited), including integrin, NCOR1, complement complex and pro-inflammatory cytokines, and chemokines (Figure S3F). Top diseases and bio-functions pointed toward engulfment, cell movement, invasion, cytoplasm organization, and Alzheimer's disease annotations (Figure S3E) with *Z* scores mostly predicting a decreased activation state. Both ITGAX and PTGS1 were found at the intersection of the proteomic and transcriptomic datasets (Figure S3G). Collectively, our multi-omics results highlighted the phagocytosis, integrin signaling, and actin cytoskeleton signaling pathways as potentially disrupted due to the lack of MECP2 protein in microglia.

The absence of MECP2 leads to alterations in microglial functions

We next moved to the analysis of microglial functions associated with the converging molecular pathways found in various datasets, such as cell movement, neuroinflammation, and phagocytosis, beginning by quantifying the release of several factors by MGLs into the media. Glutamate has been postulated to be a neurotoxic factor released by microglial cells during diseased conditions (Mesci et al., 2015). KO MGLs released twice as much glutamate as CTRL or KO^{R} MGLs (Figure 3A). KO MGLs also released three times more ROS compared to CTRL and KO^{R} MGLs (Figure 3B), validating our screening results of increased NADPH oxidase 4 gene expression and MECP2 ChIP-seq occupancy of the promoter of the *CYBB* gene encoding NADPH oxidase 2 (Figures 1I and 2E). Microglia sense and migrate toward chemoattractant molecules (Davalos et al., 2005; Nimmerjahn et al., 2005), and pathways associated with migration, cell invasion, and chemokine signaling were identified in transcriptomic analyses. While all three genotypes of microglia had similar chemotaxis in response to ATP, KO MGLs had decreased chemotaxis in response to fractalkine (CX3CL1) (Figure 3C), a neuronal chemoattractant that binds CX3CR1 expressed on microglial cells (Figure S1B). Microglia respond to inflammatory stimuli by secreting cytokines and chemokines (Chhor et al., 2013; Orihuela et al., 2016). Thus, we measured levels of 26 cytokines and chemokines released by unstimulated MGLs and those stimulated with pro-inflammatory lipopolysaccharides (LPSs) and anti-inflammatory IL-4 (Figures 3D–3F and S4A). Globally, all three genotypes, CTRL, KO, and KO^{R} MGLs, have similar levels of cytokine

Figure 2. MeCP2 chromatin immunoprecipitation sequencing and proteomic assays on MGL

(A) Explanatory schematic of CTRL, KO^{R}, and KO MGLs regarding the role of MeCP2.

(B) Venn diagram of MeCP2 occupation peaks between CTRL and KO^{R}.

(C) Annotation distribution of MeCP2 target peaks.

(D) Top canonical pathways for the promoter-TSS region obtained using IPA, where significance was calculated by the right-tailed Fisher's exact test ($p < 0.05$).

(E) A table highlighting several MECP2 targets of interest in the genome.

(F and G) Top 5 known and *de novo* motifs obtained with MeCP2 ChIP-seq in MGLs.

(H) LC-MS proteomic analyses conducted on MGL shows 480 overlapping candidates with MeCP2 ChIP-seq in the promoter region.

(I) Top canonical pathways of the intersecting candidates between proteomics and ChIP-seq obtained through IPA ($p < 0.05$).

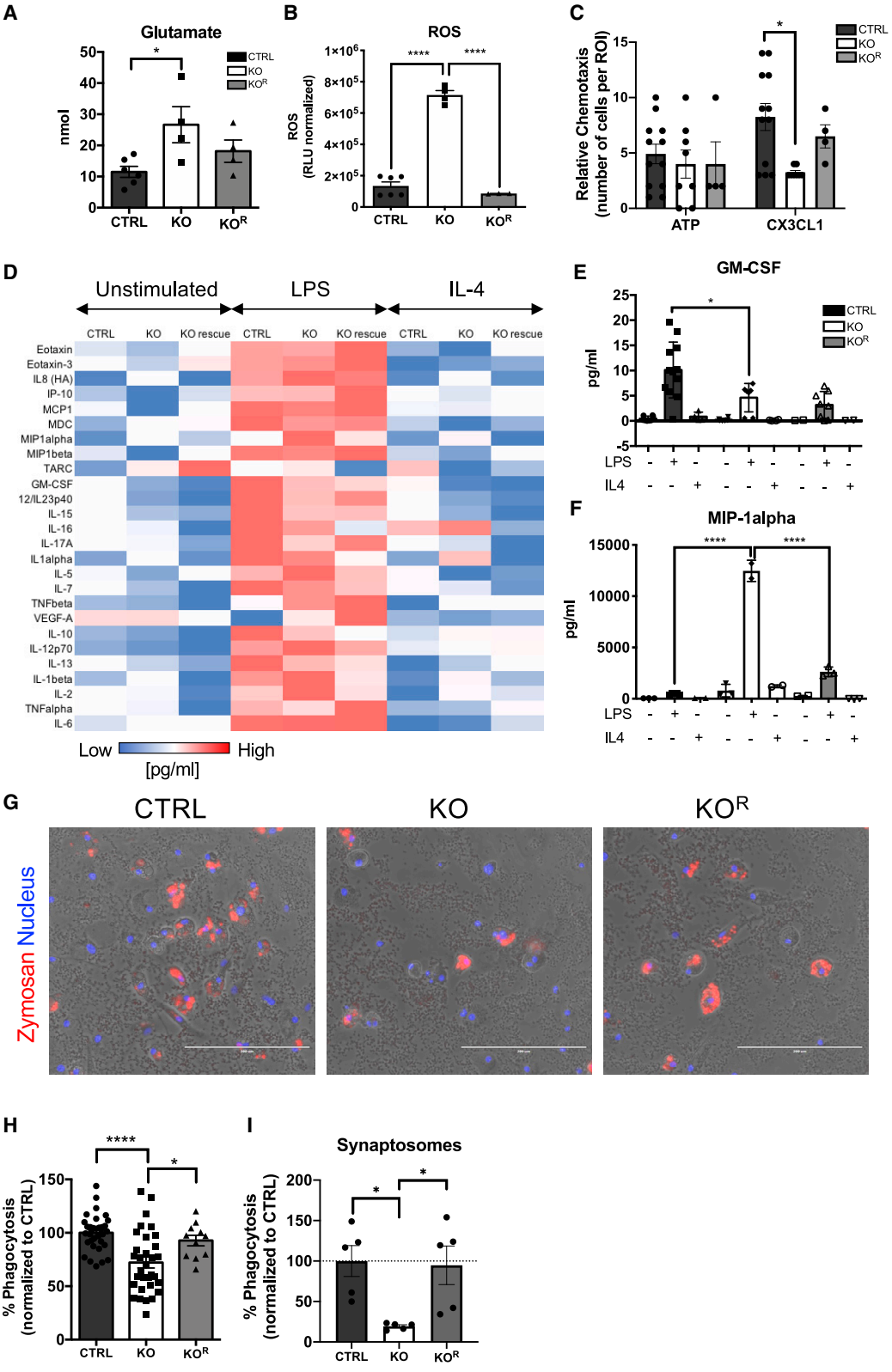

(legend on next page)

release into the media and respond similarly to both stimulations. Upon activation with LPS, the majority of pro-inflammatory cytokines release was increased. In contrast, the IL-4 stimulation had the opposite effect, suggesting that the inflammatory response to LPS or IL-4 is independent of MECP2 protein expression (Figures 3D–3F and S4A). We only noted two exceptions between KO and control MGLs; LPS-stimulated KO MGLs released significantly more Macrophage Inflammatory Protein-1 alpha (MIP-1 alpha) and less granulocyte-macrophage colony stimulating factor (GM-CSF) compared to CTRL or KO^R MGLs (Figures 3D–3F), consistent with altered MGL chemotaxis in the absence of MECP2 protein while the rest of the 26 analytes showed similar results, suggesting that MECP2 did not impact the overall immune response to LPS or IL-4 in human MGLs in our experiments.

Dysregulated phagosome formation, phagocytosis, phagosome maturation, integrin signaling, complement, and actin cytoskeleton signaling pathways were identified across all omics. Thus, we next focused on a crucial microglial function: phagocytosis. CTRL and KO^R MGLs had similar levels of phagocytic engulfment of zymosan particles, while KO MGLs showed decreased phagocytosis (Figures 3G and 3H). Upon treatment with cytochalasin D to inhibit actin polymerization, the engulfment of zymosan particles was reduced, confirming a phagocytotic process (Figures S4B–S4C). To confirm these data, we also performed phagocytosis using pHrodo-red-conjugated human brain organoid-derived cellular fractions enriched in synaptosomes (Figures 3I, S4B, and S4C). CTRL and KO^R efficiently phagocytosed synaptosomes similarly, while KO MGLs engulfed 80% less compared to CTRL and KO^R (Figure 3I).

KO^R/CTRL MGL rescues the synaptic defects when co-cultured with KO neurons

Given that several key microglial functions such as efficient phagocytosis were disrupted, we hypothesized that these functional alterations could impact neuronal development and connectivity. To address this question, we performed hiPSC-derived neuron-MGL co-culture experiments (Figures 4 and S5A–S5K). The MGLs were pre-labeled with a fluorescent membrane dye, PKH26, suitable for long-term studies, and their presence in culture was monitored during neuronal differentiation for 6–8 weeks (Figures 4A and 4B). As expected, the presence of IL-34 and macrophage colony stimulating factor (M-CSF) in the media did not alter the synaptogenesis (Figures S5D–S5E), as these ligands only bind to CSF1R, which is highly expressed by MGLs rather than neurons (Figure S5C). After 8 weeks of co-culture, the number of functional synapses defined as colocalization of pre- and post-synaptic proteins (= colocalized synaptic puncta, CSP) was counted (Figures 4C, 4D, S5D, and S5E). As we previously showed (Marchetto et al., 2010), *MECP2* KO neurons displayed 50% less CSP compared to CTRL and KO^R neurons (Figures 4C, 4D, S5D, and S5E). Adding CTRL MGLs onto CTRL neurons significantly increased the number of CSP (Figures 4C, 4D, and

Figure 3. KO MGLs have increased glutamate, and ROS release decreased phagocytosis but the globally similar inflammatory response to LPS as CTRL and KO^R MGL

(A) Glutamate release by MGLs. Bars represent mean ± SEM. Significance was tested by one-way ANOVA with Tukey's multiple comparison test (*p = 0.0329, two different KO lines, one rescue line and two independent CTRL MGL lines with two clones).

(B) Measurement of reactive oxygen species (ROS) released in the conditioned media by MGLs. One-way ANOVA with Tukey's multiple comparison test was used to assess the significance (****p < 0.0001). Bars represent mean ± SEM. Two independent cell lines for CTRL and KO MGLs and one isogenic rescue line with three independent experiments per sample were used.

(C) Migration assays using transwell chambers using ATP or CXC3L1. Significance was tested by one-way ANOVA with Tukey's multiple comparison test (*p = 0.0261), two independent cell lines for CTRL and KO MGLs, and one isogenic rescue line with three independent experiments per sample.

(D) Heatmap showing the means for each cytokine released in the conditioned media for a given genotype (blue to red, low to high concentration in the media in pg/mL), three independent CTRL and KO MGL lines and two isogenic rescue lines were used.

(E and F) MIP-1 alpha and GM-CSF released in the conditioned media by MGLs was measured, respectively (in pg/mL). Significance was tested by one-way ANOVA with Tukey's multiple comparison test (****p < 0.0001 and *p = 0.0179, three independent CTRL and KO MGL lines and two isogenic rescue lines were used). Bars represent mean ± SD.

(G) Bright-field images of CTRL, KO, and KO^R MGLs engulfing zymosan particles. Once engulfed, the zymosan particles fluoresce in red, scale bar 200 μm. Blue is a live nuclear stain (Nucleo Blue).

(H) Phagocytosis percentage of zymosan particles compared to CTRL MGLs. Significance was tested by one-way ANOVA with Tukey's multiple comparison test (****p < 0.0001 and *p = 0.0289, two different isogenic KO/KO^R pairs, at least four biological replicates each, two independent CTRL MGL lines with three clones). Bars represent mean ± SEM. Each dot represents one sample.

(I) Phagocytosis of pHrodo-conjugated brain organoid-derived synaptosomes-enriched fractions measured as red fluorescent area normalized to hour = 0 and to CTRL baseline phagocytosis using incucyte. Significance was tested by one-way ANOVA (*p < 0.001) using one control and one KO isogenic pair with 5 independent experiments each. Bars represent mean ± SEM. (*p = 0.0184 and *p = 0.0269, respectively).

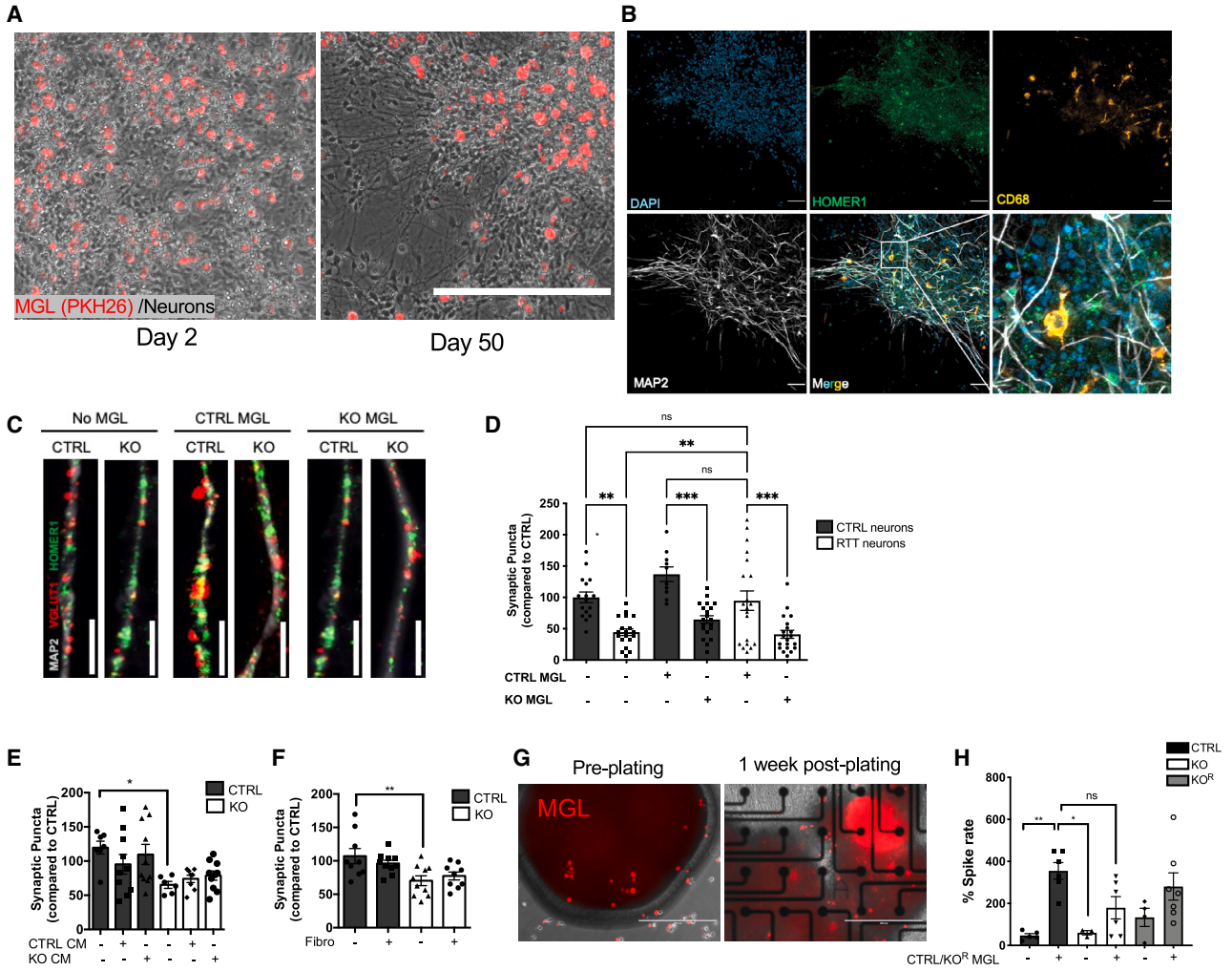

Figure 4. KO^R or CTRL MGL rescues the synaptic defects of KO neurons in long-term co-culture experiments

(A) Bright-field images of neuron-MGL (labeled with long-term stable membrane stain PKH26 in red) co-culture on day 2 and 50 of neuronal differentiation, scale bar 400 μm.

(B) Representative images of co-culture neurons (stained with MAP2 and HOMER1) and MGLs (stained with CD68) for 2 months. The last panel shows a magnification of the square area shown. Note that MGL is nearby of MAP2$^+$ neurons and synapses, scale bar 50 μm.

(C) Representative images of synaptic puncta co-localization with or without CTRL, KO, or KO^R MGLs, scale bar 20 μm.

(D) Quantification of the number of synaptic puncta (KO vs. CTRL neurons without MGL $^{**}p = 0.0013$; KO neurons without MGL vs. KO neurons with CTRL MGLs $^{**}p = 0.0023$; KO neurons with CTRL MGLs vs. KO neurons with KO MGLs $^{***}p = 0.0007$, one isogenic KO/KO^R pair [KO^R results shown in Figure.S5d], and one CTRL MGL line was used [related to KO], synaptic puncta from 10 neurons were counted, the experiment was run in two independent batches).

(E) Quantification of the number of co-localized synaptic puncta (CM, conditioned media from CTRL or KO MGLs) ($^*p = 0.0482$ one isogenic KO/KO^R pair and one CTRL MGLs line was used, synaptic puncta from 10 neurons were counted).

(F) Quantification of the number of co-localized synaptic puncta without healthy human primary fibroblasts (Fibro), ($^{**}p = 0.0084$, one isogenic KO/KO^R pair, and one CTRL MGLs line was used, synaptic puncta from 10 to 15 neurons were counted).

(G) Bright-field images of spheroids co-cultured with MGL (in red) before and after plating on MEA plates, scale bar 400 μm.

(H) Graph showing the spike rate compared to CTRL spheroids without any MGLs, recorded in 5 min emerging from spheroids with or without CTRL or KO^R MGLs. $^{**}p = 0.0021$, $^*p = 0.0150$, n.s. not significant, one isogenic rescue line and two different CTRL and KO lines were used, two to three independent experiments per genotype were used. Significance is assessed by one-way ANOVA with Tukey's multiple comparison test for the experiments in D, E, F, and H ($^*p < 0.05$, $^{**}p < 0.01$, $^{***}p < 0.001$, $^{****}p < 0.0001$). The number of neurons counted for synaptic puncta is represented by one data point in each graph. All synaptic puncta quantification was calculated as a percentage compared to CTRL neurons. Bars represent mean ± SEM.

S5A–S5D). Importantly, adding CTRL or KO^{R} MGLs onto KO neurons rescued the synaptic defects, suggesting that MECP2 re-expression in MGL is sufficient to rescue synaptogenesis (Figures 4C, 4D, S5D, and S5E). While adding CTRL/KO^{R} MGL onto KO neurons rescued the CSP, neither the number of branching points nor the neurite length changed (Figures S5F–S5G). Although there was an increase in soma size of KO neurons upon addition of MGLs, this result was not statistically significant (Figure S5G). To determine whether MGL-induced synaptogenesis required physical contact of microglia with neurons or occurred through secreted factors by microglial cells, we performed synaptogenesis assays using CTRL or KO-conditioned media from MGLs (Figures 4E, S5H, and S5J). Adding CTRL or KO MGL-conditioned media did not affect the CSP number in CTRL or KO neurons, suggesting that the effect of MGLs on neurons is mediated by cell-to-cell interactions (Figures 4E, S5H, and S5J). As a control, the addition of healthy human primary fibroblasts did not affect synaptogenesis, suggesting the results observed on neurons are microglia specific (Figures 4F, S5I, and S5K).

Finally, to assess if an increased synapse number translated into increased neuronal network activity, we performed self-assembled 3D cortical spheroid-MGL co-cultures (Figures 4G, 4H, and S5K–S5O), and we previously showed that KO cortical spheroids had decreased synchronized neuronal activity (Sharma et al., 2019). Adding CTRL MGLs onto CTRL cortical spheroids significantly increased the spike rate and the number of spikes, in agreement with the observed increased number of CSP (Figures 4G, 4H, and S5L–S5O). KO cortical spheroids without MGLs had lower spiking rate compared to CTRL spheroids with CTRL MGLs, but adding CTRL or KO^{R} MGLs increased their spiking rate, reverting this phenotype (Figures 4G, 4H, and S5L–S5O). However, adding CTRL or KO^{R} MGLs onto CTRL, KO^{R}, or KO spheroids did not change the burst duration, number of spikes per burst, number of active electrodes, or number of bursts (Figure S5O). Collectively, our data revealed that CTRL/KO^{R} MGLs rescued the synaptic defects observed in cortical neurons lacking MECP2, both at the level of the number of CSP and neuronal activity (Figures 4G, 4H, and S5L–S5O).

ADH-503 restored phagocytosis in KO MGLs, synaptic defects in KO neurons, improves disease course and survival of MeCP2 KO mice

Next, we performed a therapeutic compound screening to rescue that function and to help us understand the mechanisms by which MECP2 controls phagocytosis (Figures 3H, 3I, and S4C). We chose 8 compounds that were either inhibitors or agonists of different integrin and complement system that we previously identified (Figures 2, 3, and 5A). Among these compounds, we identified ADH-503, a CD11b agonist, for which the gene encoding for CD11b, *ITGAM*, is one of the targets for MECP2 occupancy (Figures 2E, 5C, and 5D), that was able to rescue the phagocytosis in KO MGL (Figure 5B). Next, we treated KO spheroid-MGLs co-cultures with ADH-503 (Figures 5E and S5). ADH-503 treatment of KO spheroid co-cultured with KO MGLs restored the synaptic defects to similar levels as control spheroids co-cultured with CTRL MGLs and KO spheroids co-cultured with CTRL MGLs (Figures 5E and S5).

To assess the translational potential of this candidate drug *in vivo*, we next used MeCP2-KO (Mecp2 tm1.1Jae) mice (Derecki et al., 2012). In addition to developing disease phenotypes as observed with the hiPSC-derived models and defects in microglial phagocytosis (Derecki et al., 2012), these mice develop similar pathologies seen in patients with Rett syndrome (RTT), including the nervous system and peripheric symptoms (behavior, respiratory problems, premature aging/death, etc.) (RZ et al., 2001). Therefore, we next treated MeCP2-KO mice starting at 3 weeks of age daily by oral gavage with 120 mg/kg ADH-503, a dose (half-life of 4.68 and 3.95 h) and administration route previously known to be safe (Panni et al., 2019a; Figure 5F). MeCP2-KO mice that received ADH-503 daily showed slowed disease progression (Figure 5G) and, importantly, survived 40% longer than the ones that received the vehicle treatment (Figure 5H). Finally, the MeCP2-KO mice that were treated with ADH-503 had their soma size rescued to the wild-type (WT) proportions (Figure 5I), suggesting that ADH-503 had an impact on the CNS.

DISCUSSION

Our work provides direct experimental evidence that MGL is causally involved in human synaptogenesis and neural network establishment. Not only has microglial identity been shown to be heavily defined by their neuronal environment (Bennett and Bennett, 2020; Butovsky et al., 2014; Reemst et al., 2016; Sellgren et al., 2019), but also our results suggest that microglia impact the function and maturation of neuronal cells in a human model, revealing a previously underappreciated non-cell-autonomous role of microglia on neuronal connectivity and synapse formation.

To further understand the contribution of human MGLs to disease states, we took advantage of the similarities between FM and MGLs regarding the levels of ASD-related gene expression. We observed morphological alterations and a latency period in the MGL generation from KO samples. Interestingly, a previous study reported that the myeloid-specific transcriptional factor PU.1, which we

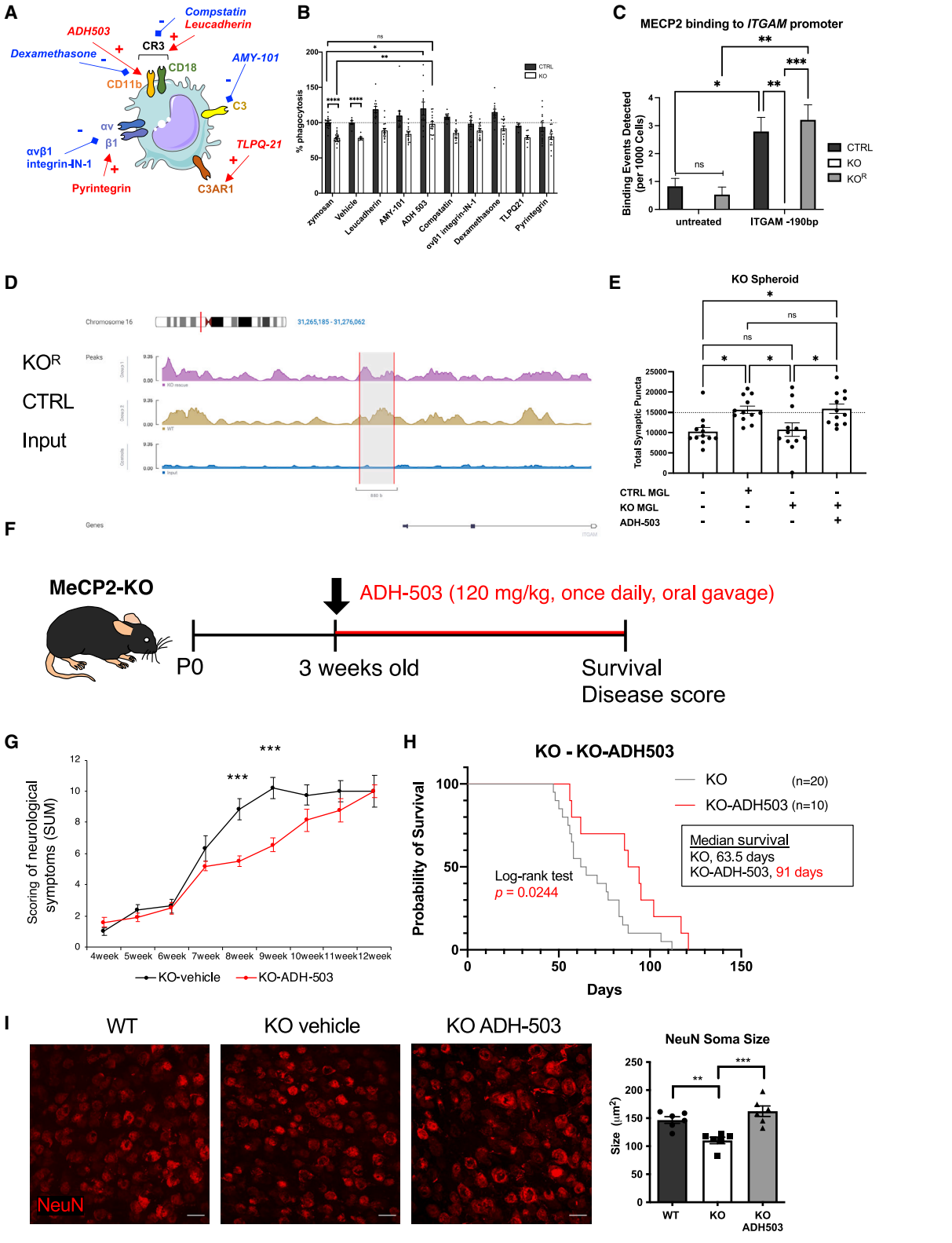

(legend on next page)

also identified as one of the top 5 known binding motif sites for microglial MECP2 in our ChIP-sequencing experiments, directly interacts with MECP2 (Suzuki et al., 2003), suggesting that MECP2 might also play a role during primitive hematopoiesis.

Our multi-omics repeatedly showed that several microglial functions, such as phagocytosis, migration, and neuroinflammation signaling pathways, could be altered. KO MGLs revealed similarities to the findings in RTT mouse models, such as increased glutamate release (Maezawa and Jin, 2010), and defective phagocytosis (Derecki et al., 2012; Zhao et al., 2017). We also found that KO MGLs also had an increased ROS production and impaired chemotaxis to fractalkine and response to LPS stimulation similar to CTRL MGLs, suggesting their ability to react to an immune stimulus remains globally intact.

We established long-term co-culture systems and showed that CTRL/KO^{R} MGLs functionally rescued the synaptogenesis defect of MECP2-lacking neurons. Neurite branching or length was not rescued, indicating a specific role in synapse formation. In contrast to mouse studies (Maezawa and Jin, 2010), human MGL-conditioned media alone did not impact CSP numbers, suggesting that the molecules secreted from KO MGL are not sufficient to elicit changes in CSP. Instead, our data showed that signaling pathways, such as integrin, chemokine, actin cytoskeleton, and complement signaling, might explain how CTRL MGL rescues the synaptic defects in MECP2 KO neurons. These data also indicate that adding KO MGLs could have a deleterious effect on synaptogenesis.

Phagocytosis is a complex receptor-mediated process that requires three main parts, "find-me," "eat-me," and "digest-me," each of which in turn is regulated by different receptors, molecules, and signaling pathways. Although recent studies have begun to focus on microglial phagocytosis in adult neurological disorders (Galloway et al., 2019; Garcia-Reitboeck et al., 2018; Sellgren et al., 2019), the contribution of microglial engulfment to human neurodevelopmental conditions has been largely unexplored. We found alterations at each step of the phagocytosis process in KO MGLs. Interestingly, microglial phagocytosis has been previously shown to be important in mouse models of RTT (Derecki et al., 2012). By using phagocytosis as a therapeutic target, we tested several compounds known to be agonists or inhibitors of different complement receptors or integrins involved in the process of phagocytosis. Even though we performed a small targeted drug screen, we identified one compound, ADH-503, able to restore the phagocytic function in KO MGLs and synaptic defects in KO spheroids. ADH-503 is an agonist of CD11b, which, together with CD18, forms the CR3 (Hong et al., 2016; Le Cabec et al., 2002; Stevens et al., 2007; Vivanti et al., 2020, n.d.). We have also shown that MECP2 occupies the *ITGAM* promoter, the gene encoding for CD11b. ADH-503 is a small molecule that can partially activate CD11b, which was previously developed and used as a

Figure 5. ADH-503 rescues phagocytosis in KO MGLs and synaptic defects in KO spheroids and improves disease score and survival in mouse

(A) Schematic of the compounds used in the screening; agonist compounds are in red and inhibitors in blue.

(B) Drug screening using phagocytosis assay. Phagocytosis percentage of zymosan particles compared to CTRL MGLs. Significance was tested by two-way ANOVA (****$p < 0.001$, *$p = 0.0109$, **$p = 0.0041$), experiment run in two batches, $n = 12$ to 24 biological replicates. Bars represent mean ± SEM.

(C) MECP2 binding events to *ITGAM* (CD11b) promoter, baseline binding events detected (untreated) or at the promoter region of *ITGAM*. Significance was tested by two-way ANOVA followed by Sidak multiple comparison test (***$p = 0.0004$, *$p = 0.0236$, CTRL vs. KO ITGAM -190 bp **$p = 0.0013$, untreated KO^{R} vs. *ITGAM* -190 bp **$p = 0.0019$), $n = 3$ independent experiments. Bars represent mean ± SEM.

(D) Peaks detected in the promoter region of *ITGAM* in CTRL and KO^{R} MGLs by MECP2 ChIP-seq.

(E) Quantification of colocalized synaptic (VGLUT/HOMER1) puncta in KO spheroids co-cultured with KO or CTRL MGLs and treated with 1 μM of ADH-503 using Imaris software. The dotted line indicates the number of colocalized synaptic puncta in CTRL spheroids co-cultured with CTRL MGLs. Significance was tested by one-way ANOVA with Tukey's multiple comparison test (KO no MGL vs. KO + CTRL MGLs *p = 0.0163, KO no MGL vs. KO + KO MGLs+ ADH-503 *$p = 0.0109$, KO + KO MGLs vs. KO + CTRL MGLs *$p = 0.0344$, KO + KO MGLs vs. KO + KO + ADH-503 *$p = 0.0236$, KO + CTRL MGLs vs. KO + KO MGLs+ ADH-503, and KO no MGL vs. KO + KO MGLs were non-significant).

(F) Schematic of ADH-503 treatment of MeCP2-KO male mice.

(G) Average total symptom score was calculated in each group at indicated time points. MeCP2-KO mice treated with ADH-503 showed a significant reduction in total score compared with vehicle-treated *Mecp2*-KO mice. N = KO-vehicle: 11, KO-ADH-503: 10. Significance was tested with Student's t test, week 8; ***$p = 0.0004$, week 9, ***$p = 0.0007$.

(H) Kaplan-Meier survival curves. MeCP2-KO mice treated with ADH-503 survived significantly longer than non-treated control MeCP2-KO mice (*$p = 0.0244$; log rank test), with median survival of 63.5 days (for control mice) and 91 days (for ADH-503-treated mice). N = KO: 20, KO-ADH-503: 10.

(I) Cryosections of WT or MeCP2-KO mouse brains treated with vehicle or ADH-503 stained with NeuN (scale bar 100 μm, on the left) and measurement of soma size was plotted on a bar graph. Significance was tested by one-way ANOVA with Tukey's multiple comparison test (**$p = 0.0078$, ***$p = 0.0004$), $n = 6$ mice/group.

treatment for pancreatic cancer and is currently in phase 1 of clinical trials (Panni et al., 2019b). Daily treatment of MeCP2-KO mice, similar to our *in vitro* studies using patient-derived cell lines to improve clinical translation of this study, whose microglial phagocytosis is also altered (Derecki et al., 2012), with ADH-503 led to a significant improvement of the symptom progression and increased survival. Moreover, it is important to note that despite the treatment starting at 3 weeks, hence after disease onset, the treatment is still able to significantly improve the progression of the disease. Apart from rescuing neuronal soma size, ADH treatment might improve the overall symptoms of the mice by acting on peripheral macrophages/other myeloid cells that also express CD11b and were shown to have altered phenotypes in RTT mouse models (Cronk et al., 2015; Schafer and Stevens, 2015). However, given that RTT is mainly considered a disease in females since it is X-linked, additional studies should be performed using female cell lines and female RTT mouse models.

Our data revealed that MECP2 is required for microglial functions such as phagocytosis, likely through CD11b, and support that MGL plays a role in human neurodevelopment, notably in synapse formation (Derecki et al., 2012; Garré et al., 2020; Schafer et al., 2016). We also found some differences with rodent models regarding inflammation and the role of secreted factors on neurotoxicity (Cronk et al., 2015; Maezawa and Jin, 2010), highlighting the importance of using a human model to understand the disease-relevant mechanisms. Improving the generation of hiPSC-derived microglial surrogates to replace the unhealthy host microglia could represent a starting point for cell-based therapies (Bennett and Bennett, 2020).

Our findings establish the experimental groundwork to identify molecules involved in human neuro-immune interactions during development. A better understanding of the molecular and cellular interplay between neurons and microglia in a human experimental model could provide a better understanding of microglia in physiological conditions during neurodevelopment. Our results provide initial clinical evidence that *human microglial cells could be used as therapeutic targets* that can lead to the discovery of novel and efficient treatments for uncurable neurological disorders. Given that microglial cells are immune cells of the CNS, implicated in all neurological conditions, focusing on studying microglial disease phenotypes and performing drug screenings specifically to rescue altered microglial phenotypes could pave the way to innovative treatments for neurodevelopmental but also broader neurological conditions. Although microglial cells may not be the initial disease-driving cell type in most neurological conditions, identification of disease pathways in human microglial cells offers a unique opportunity to be able to intervene during symptomatic phases/after the onset of any given neurological disorder where these cells play a pivotal role. One of the main issues in the treatment of neurological conditions is the lack of clear disease onset biomarkers and prediction methods to intervene before disease onset. Therefore, current treatment options for patients are offered once the symptoms appear and continue developing, which is often too late to target the initial victim cell type and/or disease mechanism. Thus, targeting microglial cells, which are implicated in the symptomatic phases of the disease, to identify new therapeutic targets may give the patients a fighting chance to improve or even overcome their conditions.

EXPERIMENTAL PROCEDURES

Resource availability

Lead contact

Further information and requests for resources and reagents should be directed to and will be fulfilled by the lead contact, Pinar Mesci (pmesci@gmail.com).

Materials availability

This study did not generate new unique reagents. Extended detailed experimental procedures can be found in the supplemental information section.

Data and code availability

The data that support the findings of this study are available from the corresponding author upon reasonable request. ChIP-seq and RNA-seq data are all available under NCBI-BioProject ID PRJNA635136.

Phagocytosis assay

Phagocytosis assay was performed according to the manufacturer's instructions with pHrodo Red Zymosan A BioParticles (Life Technologies, Carlsbad, USA) conjugate for phagocytosis. Briefly, 20,000 MGLs were plated on a 96-well tissue culture plate and incubated in M2 media (Neurobasal media supplemented with 2× Gem21 NeuroPlex, 1× NEAA, 1× GlutaMAX) containing fluorescently labeled zymosan particles (0.125 mg/mL) for 2 h at 37°C, 5% CO_2. Fluorescence was measured with Tecan Infinite 200 PRO microplate reader (Life Sciences, Switzerland).

For experiments featuring block of zymosan uptake, cell monolayers were treated with 1 μM Cytochalasin D (Sigma-Aldrich) 30 min prior to incubation with zymosan.

For the compound screening, MGLs were pre-treated with each compound 1 day prior to the phagocytosis assay. All compounds were used at 10 μM, which did not cause any decrease in cell viability.

Brain cortical organoid-derived synaptosome-enriched fraction isolation

Synaptosomes were isolated from 6-week-old brain organoids from CTRL samples generated from our previously published protocol (Trujillo et al., 2018) (using Syn-PER Synaptic Protein Extraction Reagent (Thermo Fisher Scientific) according to the manufacturer's instructions. Synaptosomes were then conjugated using IncuCyte

pHrodo Red Cell Labeling Kit for phagocytosis and added on top of MGLs for 2 h. The fluorescence was measured using the Incucyte software.

Glutamate assay

The Glutamate Colorimetric Assay kit (ab83389, Abcam, USA) was used to measure the glutamate in the conditioned media by MGLs following the manufacturer's instructions. 50,000 MGLs were plated in 100 μL of media and conditioned for 24 h. 50 μL of samples was used.

ROS assay

50,000 MGLs were plated in 100 μL of media and conditioned for 24 h. ROS-Glo H_2O_2 Assay (Promega, USA) was used to measure the ROS in the conditioned media by MGLs according to the manufacturer's instructions. The relative luminescence unit was recorded in a plate reader.

Image analysis

ImageJ software was used to calculate the integrated density of MeCP2 (antibody information is provided further in immunocytochemistry section) in MGL. Briefly, the channels were split and the integrated density of the appropriate channel was measured by the software as previously described (Zhu et al., 2020).

Chemotaxis assay

Chemotaxis assay was performed using 5 μm polyester transwell chamber, with 300 mM ATP or CX3CL1 at 100 ng/mL for 4 h. The cells that have migrated through the chamber were then manually counted in several regions of interest.

Immunocytochemistry

Mice were anesthetized and perfused *trans*-cardiac with PBS followed by 4% buffered paraformaldehyde (PFA) at 8 weeks. Brains were removed and fixed with 4% PFA overnight at 4°C. The fixed tissue was cryoprotected with 30% sucrose and frozen in optimal cutting temperature medium. Coronal sections were obtained by sectioning the tissue at 30 μm using a microtome. The images were taken in the hippocampal CA1 region in the cerebral cortex similar to previous studies (Derecki et al., 2012). Soma was visualized using NeuN staining; each NeuN+ soma was measured by manual tracing using ImageJ software.

MGLs, neuron-MGL, neuron-fibroblast, and neurons with MGL-conditioned media were fixed with 4% PFA for 20 min at room temperature. Cells were permeabilized and incubated with blocking solution (10% fetal bovine serum [Life Technologies], 0.1% [v/v] Triton X-100 in 1× Dulbecco's phosphate buffer solution [DPBS, Gibco]) for 30 min. Then, the primary antibody was added (diluted in blocking solution) and samples were incubated overnight at 4°C. Cells were then washed two times with 1×-PBS and incubated with the secondary antibody for 1 h at room temperature. Secondary antibodies (all conjugated to Alexa Fluor 488, 555, and 647) were purchased from Life Technologies and used at a 1:1,000 dilution. Cells were washed twice (1x-PBS), incubated with fluorescent nuclear 6-diamidino-2-phenylindole (DAPI, VWR International, 1:5,000) for 10 min, and mounted with Prolong gold anti-fade reagent (Life Technologies). Samples were imaged using an Axio Observer Z1 Microscope with ApoTome (Zeiss).

Antibodies and dilutions used: monoclonal mouse anti-human CD68, (1:500, Dako); polyclonal rabbit anti-Iba-1, (1:500, Wako), polyclonal rabbit anti-human PU.1 (1:500, Cell Signaling Technology), polyclonal rabbit anti-CX3CR1 (1:2,000, Bio-Rad), polyclonal goat anti-human TREM2 (1:100, R&D Systems), monoclonal mouse anti-human CD11b (1:500, BD Biosciences), polyclonal rabbit anti-human P2YR12 (1:125, Alomone), polyclonal rabbit anti-human MeCP2 (1:500, Diagenode), anti-Homer1 (Synaptic Systems, 1:500), anti-VGLUT1 (Synaptic Systems, 1:500), anti-MAP2 (Abcam, 1:2,000), and NeuN (Millipore, 1:500).

Co-culture experiments

For neuron-MGL or primary control fibroblast co-culture experiments, we plated 50,000 NPCs on PO-Laminin-coated coverslips in NPC media (see above). The next day, we retrieved the basic Fibroblast Growth Factor (bFGF) and added Rock inhibitor to start neuronal differentiation. 50,000 MGL progenitor cells freshly sorted with $CD14^+$ microbeads or 50,000 primary fibroblasts were directly added onto each coverslip. The neurons were allowed to differentiate for 6–8 weeks in the presence of MGL or fibroblast before proceeding with the synaptogenesis assays. The fibroblasts and the MGL were first labeled with the membrane dye PKH26 to verify their presence at the end of the 8 weeks of neuronal differentiation. Then, another batch of co-culture was generated, this time without the membrane dye, to be able to perform the immunostainings for synaptic proteins without interference from the fluorescent dye. Finally, for neurons with MGL conditioned media, we plated 50,000 MGLs per 96-well plate and conditioned media for 48 h in neuronal media (see above) supplemented with 50 ng/mL IL-34 and 50 ng/mL M-CSF. Conditioned media from each well were recovered, filtered using 40 μm cell strainer (BD Biosciences). 100 μL of filtered MGL conditioned media was added onto each coverslip with neurons every 2 days for 6–8 weeks.

Synapse formation assay

hiPSC-derived neurons co-cultured with MGL, fibroblasts, or with MGL-conditioned media were fixed at 6–8 weeks after bFGF retrieval and imaged using an Axio Observer Z1 Microscope with Apotome (Zeiss) using compiled z stack images at an objective resolution of 63X. Co-localization of pre- (VGLUT1) and post-synaptic (HOMER1) markers were quantified manually when in contact with MAP2 at a length of 50 μm as previously described (Derecki et al., 2012). Each co-culture combination had at least 10 to 15 images processed from which 10 to 20 MAP2-positive neurons were used for co-localized synaptic puncta quantification from a total of four biological replicated and two independent co-cultured batches. For drug-treated 3D-MGL spheroid cultures, 7 days after initial spheroid plating, high-resolution images were captured using a Dragonfly microscope, employing z stack imaging with a 40× objective resolution. Subsequently, co-localization analysis of pre-synaptic (VGLUT1 1:500, Cat.No. 135 311 – Synaptic Systems antibodies) and post-synaptic (HOMER1 1:500, Cat.No. 160

003 – Synaptic Systems antibodies) markers in conjunction with MAP2 (1:2,000, PA1-10005 -Invitrogen) was quantified utilizing the Imaris 10.1 software (Oxford Instruments). Notably, each co-culture combination underwent rigorous analysis, with a minimum of 12 images processed per combination, ensuring comprehensive and statistically robust data collection. To analyze the data, the number of HOMER1 and VGLUT1 dots was quantified, along with the volume of axons measured in cubic micrometers (μm^3). Subsequently, we assessed the colocalization of HOMER1 points with the axons. Next, we quantified the colocalization of VGLUT1 points with both HOMER1 and axons. The data were then normalized using the following equation. Finally, the data were represented as the density of HOMER1/VGLUT normalized by the volume of the axons measured in cubic micrometers (μm^3).

$$\frac{(Number\ of\ colocalized\ VGlut1\ puncta)}{Total\ number\ of\ VGlut\ puncta} * \frac{1}{Total\ volume\ og\ Axons\ in\ \mu m^3}$$

Neurite tracing

Images used for neurite tracing were taken from an Axio Observer Z1 Microscope with Apotome (Zeiss) using compiled z stack images at an objective resolution of 63X. iPSC-derived neurons were immunostained using microtubule-associated protein 2 (MAP2) as a neuronal marker to indicate neurite outgrowth. MAP2-positive neurites were then manually traced using the software, ImageJ, with the plugin extension, NeuronJ. Manual traces began at the starting point of the MAP2-positive neurite and were followed along the path until where the neurite terminates. Branches were traced in the same way. Distance was calibrated at a scale of 9.757 pixels/μm.

Mesoscale assay

$CD14^+$-sorted iPSC-derived MGLs were seeded at 5×10^4 cells per well on 96-well cell culture plates and kept in M2 media. Cells were stimulated with or without treatments of 1 μg/mL *E. coli* LPS (Sigma-Aldrich) for 30 h. 100 μL of conditioned media was recovered from each well the next day. Cytokine levels were quantified using a customized V-PLEX Human Cytokine 30-Plex Kit (Meso Scale Discovery, Rockville, Maryland, USA) according to the manufacturer's instructions. Chemokines and cytokines measured from custom multiplex panels consist of eotaxin, eotaxin-3, IL-8 (HA), IP-10, MCP-1, MDC, MIP-1α, MIP-1β, TARC, GM-CSF, IL-12/IL-23p40, IL-15, IL-16, IL-17A, IL-1α, IL-5, IL-7, TNF-β, VEGF-A, IL-10, IL-12p70, IL-13, IL-1β, IL-2, TNF-α, and IL-6. Samples with or without LPS stimulation underwent a 10-fold or 2-fold dilution, respectively.

Statistical analyses

Results were analyzed using Prism Software (version 6, GraphPad, USA). Statistical significance was determined using one-way ANOVA tests followed by Tukey or Sidak multiple comparisons tests to compare different groups with one variable, or two-way ANOVA tests when there were two variables and Student's t test to compare means of two groups using a $p < 0.05$. The reported values are means ± SEM, as mentioned in relevant figure captions. Sample sizes, *n*, are reported in relevant figures (as data points) or figure legends.

SUPPLEMENTAL INFORMATION

Supplemental information can be found online at https://doi.org/10.1016/j.stemcr.2024.06.013.

ACKNOWLEDGMENTS

The authors are grateful to Dr. Elsa Molina of the UC San Diego Stem Cell Genomics Core for technical assistance with experiments using the NanoString nCounter Sprint. We would like to thank Dr. Amir Gamliel for helpful discussions regarding MeCP2 chromatin immunoprecipitation sequencing, the members of the Kaufman Lab (UC San Diego) for their help with the synaptosome phagocytosis assays, Bryan S. Kerwin and Bryan Walker from Animantis, LLC (San Diego, USA) for their help with microglia-like cells' morphometrics, the UC San Diego Biomolecular and Proteomics Mass Spectrometry Facility (BPMSF) and finally Jean Lozach from Rosalind OnRamp (San Diego, USA), and Dr. Angels Almenar-Queralt for critical reading of the manuscript. This work was made possible in part by the CIRM Major Facilities grant (FA1-00607) to the Sanford Consortium for Regenerative Medicine. A.R.M. is supported by the National Institutes of Health R01MH107367, R01HD107788, R01NS105969, and R01NS123642 and a grant from the International Rett Syndrome Foundation (IRSF). This work was also partially funded by the International Rett Syndrome Foundation, Innovation Award granted to P.M. (grant #3905). R.H.H. is funded by Fundação Araucária (grant #FA09/2016). This work was also partially funded by AMED (JP22mg1310008) and an Intramural Research Grant (3–9) for Neurological and Psychiatric Disorders of NCNP grant to K.N. and the Japan Society for the Promotion of Science (JSPS) KAKENHI (JP22K15201) to H.N. This publication includes data generated at the UC San Diego IGM Genomics Center utilizing an Illumina NovaSeq 6000 that was purchased with funding from a National Institutes of Health SIG grant (#S10 OD026929).

AUTHOR CONTRIBUTIONS

P.M. and A.R.M. conceived this study. P.M. designed the experiments, analyzed the data, and generated the protocols to generate microglia-like cells, as well as all co-culture experiments. C.N.L. and V.N. helped with the phagocytosis and migration assays and provided scientific input. J.J.J. contributed to the microglia-like cell generation and helped with synaptogenesis, neurite tracing, and mesoscale assays. A.F. and R.H.H. helped with the analyses of chromatin immunoprecipitation sequencing, proteomics, and bulk RNA sequencing. A.S. helped with ROS experiments. G.G. and C.E.S. helped with iPSC cultures and immunocytochemistry experiments. N.C. and S.S. helped with spheroid microglia co-culture experiments. H.N. and K.N. performed the mouse experiments. T.O. helped with data analyses of mouse experiments. C.A.T. generated two isogenic cell lines. P.M. and A.R.M. interpreted the results and wrote the manuscript. All authors revised, contributed, and approved the final manuscript.

DECLARATION OF INTERESTS

A.R.M. is a co-founder and has an equity interest in TISMOO, a company dedicated to genetic analysis and human brain

organogenesis focusing on therapeutic applications customized for the disorder autism spectrum and other neurological disorders origin genetics. The terms of this arrangement have been reviewed and approved by the University of California, San Diego, in accordance with its conflict-of-interest policies.

The authors have a patent application in works related to this publication.

Received: July 4, 2023
Revised: June 27, 2024
Accepted: June 28, 2024
Published: July 25, 2024

REFERENCES

Alliot, F., Godin, I., and Pessac, B. (1999). Microglia derive from progenitors, originating from the yolk sac, and which proliferate in the brain. Brain Res. Dev. Brain Res. *117*, 145–152. http://www.ncbi.nlm.nih.gov/pubmed/10567732.

Barski, A., Cuddapah, S., Cui, K., Roh, T.Y., Schones, D.E., Wang, Z., Wei, G., Chepelev, I., and Zhao, K. (2007). High-Resolution Profiling of Histone Methylations in the Human Genome. Cell *129*, 823–837. https://doi.org/10.1016/j.cell.2007.05.009.

Bennett, M.L., and Bennett, F.C. (2020). The influence of environment and origin on brain resident macrophages and implications for therapy. Nat. Neurosci. *23*, 157–166. https://doi.org/10.1038/s41593-019-0545-6.

Beyer, K.S., Blasi, F., Bacchelli, E., Klauck, S.M., Maestrini, E., and Poustka, A.; International Molecular Genetic Study of Autism Consortium IMGSAC (2002). Mutation analysis of the coding sequence of the MECP2 gene in infantile autism. Hum. Genet. *111*, 305–309. https://doi.org/10.1007/s00439-002-0786-3.

Butovsky, O., Jedrychowski, M.P., Moore, C.S., Cialic, R., Lanser, A.J., Gabriely, G., Koeglsperger, T., Dake, B., Wu, P.M., Doykan, C.E., et al. (2014). Identification of a unique TGF-β-dependent molecular and functional signature in microglia. Nat. Neurosci. *17*, 131–143. https://doi.org/10.1038/nn.3599.

Cardona, A.E., Pioro, E.P., Sasse, M.E., Kostenko, V., Cardona, S.M., Dijkstra, I.M., Huang, D., Kidd, G., Dombrowski, S., Dutta, R., et al. (2006). Control of microglial neurotoxicity by the fractalkine receptor. Nat. Neurosci. *9*, 917–924. https://doi.org/10.1038/nn1715.

Chahrour, M., Sung, Y.J., Shaw, C., Zhou, X., Wong, S.T.C., Qin, J., and Zoghbi, H.Y. (2008). MeCP2, a key contributor to neurological disease, activates and represses transcription. Science *320*, 1224–1229. https://doi.org/10.1126/science.1153252.

Chao, H.-T., Zoghbi, H.Y., and Rosenmund, C. (2007). MeCP2 controls excitatory synaptic strength by regulating glutamatergic synapse number. Neuron *56*, 58–65. https://doi.org/10.1016/j.neuron.2007.08.018.

Cheung, A.Y.L., Horvath, L.M., Grafodatskaya, D., Pasceri, P., Weksberg, R., Hotta, A., Carrel, L., and Ellis, J. (2011). Isolation of MECP2-null Rett Syndrome patient hiPS cells and isogenic controls through X-chromosome inactivation. Hum. Mol. Genet. *20*, 2103–2115. https://doi.org/10.1093/hmg/ddr093.

Chhor, V., Le Charpentier, T., Lebon, S., Oré, M.-V., Celador, I.L., Josserand, J., Degos, V., Jacotot, E., Hagberg, H., Sävman, K., et al. (2013). Characterization of phenotype markers and neuronotoxic potential of polarised primary microglia in vitro. Brain Behav. Immun. *32*, 70–85. https://doi.org/10.1016/j.bbi.2013.02.005.

Colantuoni, C., Jeon, O.H., Hyder, K., Chenchik, A., Khimani, A.H., Narayanan, V., Hoffman, E.P., Kaufmann, W.E., Naidu, S., and Pevsner, J. (2001). Gene expression profiling in postmortem Rett Syndrome brain: differential gene expression and patient classification. Neurobiol. Dis. *8*, 847–865. https://doi.org/10.1006/nbdi.2001.0428.

Cronk, J.C., Derecki, N.C., Ji, E., Xu, Y., Lampano, A.E., Smirnov, I., Baker, W., Norris, G.T., Marin, I., Coddington, N., et al. (2015). Methyl-CpG Binding Protein 2 Regulates Microglia and Macrophage Gene Expression in Response to Inflammatory Stimuli. Immunity *42*, 679–691. https://doi.org/10.1016/j.immuni.2015.03.013.

Davalos, D., Grutzendler, J., Yang, G., Kim, J.V., Zuo, Y., Jung, S., Littman, D.R., Dustin, M.L., and Gan, W.-B. (2005). ATP mediates rapid microglial response to local brain injury in vivo. Nat. Neurosci. *8*, 752–758. https://doi.org/10.1038/nn1472.

Derecki, N.C., Cronk, J.C., Lu, Z., Xu, E., Abbott, S.B.G., Guyenet, P.G., and Kipnis, J. (2012). Wild-type microglia arrest pathology in a mouse model of Rett syndrome. Nature *484*, 105–109. https://doi.org/10.1038/nature10907.

Galloway, D.A., Phillips, A.E.M., Owen, D.R.J., and Moore, C.S. (2019). Phagocytosis in the Brain: Homeostasis and Disease. https://doi.org/10.3389/fimmu.2019.00790.

Gandal, M.J., Zhang, P., Hadjimichael, E., Walker, R.L., Chen, C., Liu, S., Won, H., Van Bakel, H., Varghese, M., Wang, Y., et al. (2018). Transcriptome-wide isoform-level dysregulation in ASD, schizophrenia, and bipolar disorder. Science *362*, eaat8127. https://doi.org/10.1126/science.aat8127.

Garcia-Reitboeck, P., Phillips, A., Piers, T.M., Villegas-Llerena, C., Butler, M., Mallach, A., Rodrigues, C., Arber, C.E., Heslegrave, A., Zetterberg, H., et al. (2018). Human Induced Pluripotent Stem Cell-Derived Microglia-Like Cells Harboring TREM2 Missense Mutations Show Specific Deficits in Phagocytosis. Cell Rep. *24*, 2300–2311. https://doi.org/10.1016/j.celrep.2018.07.094.

Garré, J.M., Silva, H.M., Lafaille, J.J., and Yang, G. (2020). P2X7 receptor inhibition ameliorates dendritic spine pathology and social behavioral deficits in Rett syndrome mice. Nat. Commun. *11*, 1–13. https://doi.org/10.1038/s41467-020-15590-5.

Ginhoux, F., Greter, M., Leboeuf, M., Nandi, S., See, P., Gokhan, S., Mehler, M.F., Conway, S.J., Ng, L.G., Stanley, E.R., et al. (2010). Fate mapping analysis reveals that adult microglia derive from primitive macrophages. Science *330*, 841–845. https://doi.org/10.1126/science.1194637.

Guy, J., Hendrich, B., Holmes, M., Martin, J.E., and Bird, A. (2001). A mouse Mecp2-null mutation causes neurological symptoms that mimic Rett syndrome. Nat. Genet. *27*, 322–326. https://doi.org/10.1038/85899.

Hong, S., Beja-Glasser, V.F., Nfonoyim, B.M., Frouin, A., Li, S., Ramakrishnan, S., Merry, K.M., Shi, Q., Rosenthal, A., Barres, B.A., et al. (2016). Complement and microglia mediate early synapse loss in

Alzheimer mouse models. Science *352*, 712–716. https://doi.org/10.1126/science.aad8373.

Horiuchi, M., Smith, L., Maezawa, I., and Jin, L.-W. (2017). CX3CR1 ablation ameliorates motor and respiratory dysfunctions and improves survival of a Rett syndrome mouse model. Brain Behav. Immun. *60*, 106–116. https://doi.org/10.1016/j.bbi.2016.02.014.

Jiang, M., Ash, R.T., Baker, S.A., Suter, B., Ferguson, A., Park, J., Rudy, J., Torsky, S.P., Chao, H.-T., Zoghbi, H.Y., and Smirnakis, S.M. (2013). Dendritic arborization and spine dynamics are abnormal in the mouse model of MECP2 duplication syndrome. J. Neurosci. *33*, 19518–19533. https://doi.org/10.1523/JNEUROSCI.1745-13.2013.

Jin, L.-W., Horiuchi, M., Wulff, H., Liu, X.-B., Cortopassi, G.A., Erickson, J.D., and Maezawa, I. (2015). Dysregulation of Glutamine Transporter SNAT1 in Rett Syndrome Microglia: A Mechanism for Mitochondrial Dysfunction and Neurotoxicity. J. Neurosci. *35*, 2516–2529. https://doi.org/10.1523/JNEUROSCI.2778-14.2015.

Kim, K.-Y., Hysolli, E., and Park, I.-H. (2011). Neuronal maturation defect in induced pluripotent stem cells from patients with Rett syndrome. Proc. Natl. Acad. Sci. USA *108*, 14169–14174. https://doi.org/10.1073/pnas.1018979108.

Kracht, L., Borggrewe, M., Eskandar, S., Brouwer, N., Laman, J.D., Scherjon, S.A., Prins, J.R., Kooistra, S.M., Eggen, B.J.L., and Eggen, B.J.L. (2020). Human fetal microglia acquire homeostatic immune-sensing properties early in development *369*, 530–537.

Le Cabec, V., Carréno, S., Moisand, A., Bordier, C., and Maridonneau-Parini, I. (2002). Complement Receptor 3 (CD11b/CD18) Mediates Type I and Type II Phagocytosis During Nonopsonic and Opsonic Phagocytosis, Respectively. J. Immunol. *169*, 2003–2009. https://doi.org/10.4049/jimmunol.169.4.2003.

Lioy, D.T., Garg, S.K., Monaghan, C.E., Raber, J., Foust, K.D., Kaspar, B.K., Hirrlinger, P.G., Kirchhoff, F., Bissonnette, J.M., Ballas, N., and Mandel, G. (2011). A role for glia in the progression of Rett's syndrome. Nature *475*, 497–500. https://doi.org/10.1038/nature10214.

Maezawa, I., and Jin, L.-W. (2010). Rett syndrome microglia damage dendrites and synapses by the elevated release of glutamate. J. Neurosci. *30*, 5346–5356. https://doi.org/10.1523/JNEUROSCI.5966-09.2010.

Marchetto, M.C.N., Carromeu, C., Acab, A., Yu, D., Yeo, G.W., Mu, Y., Chen, G., Gage, F.H., and Muotri, A.R. (2010). A model for neural development and treatment of Rett syndrome using human induced pluripotent stem cells. Cell *143*, 527–539. https://doi.org/10.1016/j.cell.2010.10.016.

McGraw, C.M., Samaco, R.C., and Zoghbi, H.Y. (2011). Adult neural function requires MeCP2. Science *333*, 186. https://doi.org/10.1126/science.1206593.

Menassa, D.A., and Gomez-Nicola, D. (2018). Microglial dynamics during human brain development. Front. Immunol. *9*, 1014. https://doi.org/10.3389/fimmu.2018.01014.

Mesci, P., Macia, A., LaRock, C.N., Tejwani, L., Fernandes, I.R., Suarez, N.A., Zanotto, P.M. de A., Beltrão-Braga, P.C.B., Nizet, V., and Muotri, A.R. (2018). Modeling neuro-immune interactions during Zika virus infection. Hum. Mol. Genet. *27*, 41–52. https://doi.org/10.1093/hmg/ddx382.

Mesci, P., Zaïdi, S., Lobsiger, C.S., Millecamps, S., Escartin, C., Seilhean, D., Sato, H., Mallat, M., and Boillée, S. (2015). System xC- is a mediator of microglial function and its deletion slows symptoms in amyotrophic lateral sclerosis mice. Brain *138*, 53–68. https://doi.org/10.1093/brain/awu312.

Muotri, A.R., Marchetto, M.C.N., Coufal, N.G., Oefner, R., Yeo, G., Nakashima, K., and Gage, F.H. (2010). L1 retrotransposition in neurons is modulated by MeCP2. Nature *468*, 443–446. https://doi.org/10.1038/nature09544.

Na, E.S., Nelson, E.D., Kavalali, E.T., and Monteggia, L.M. (2013). The impact of MeCP2 loss- or gain-of-function on synaptic plasticity. Neuropsychopharmacology *38*, 212–219. https://doi.org/10.1038/npp.2012.116.

Nageshappa, S., Carromeu, C., Trujillo, C.A., Mesci, P., Espuny-Camacho, I., Pasciuto, E., Vanderhaeghen, P., Verfaillie, C.M., Raitano, S., Kumar, A., et al. (2016). Altered neuronal network and rescue in a human MECP2 duplication model. Mol. Psychiatr. *21*, 178–188. https://doi.org/10.1038/mp.2015.128.

Nimmerjahn, A., Kirchhoff, F., and Helmchen, F. (2005). Resting microglial cells are highly dynamic surveillants of brain parenchyma in vivo. Science *308*, 1314–1318. https://doi.org/10.1126/science.1110647.

Orihuela, R., McPherson, C.A., and Harry, G.J. (2016). Microglial M1/M2 polarization and metabolic states. Br. J. Pharmacol. *173*, 649–665. https://doi.org/10.1111/bph.13139.

Panni, R.Z., Herndon, J.M., Zuo, C., Hegde, S., Hogg, G.D., Knolhoff, B.L., Breden, M.A., Li, X., Krisnawan, V.E., Khan, S.Q., et al. (2019a). Agonism of CD11b reprograms innate immunity to sensitize pancreatic cancer to immunotherapies. Sci. Transl. Med. *11*, eaau9240. https://doi.org/10.1126/SCITRANSLMED.AAU9240.

Panni, R.Z., Herndon, J.M., Zuo, C., Hegde, S., Hogg, G.D., Knolhoff, B.L., Breden, M.A., Li, X., Krisnawan, V.E., Khan, S.Q., et al. (2019b). Agonism of CD11b reprograms innate immunity to sensitize pancreatic cancer to immunotherapies. Sci. Transl. Med. *11*, eaau9240. https://doi.org/10.1126/scitranslmed.aau9240.

Parikshak, N.N., Swarup, V., Belgard, T.G., Irimia, M., Ramaswami, G., Gandal, M.J., Hartl, C., Leppa, V., Ubieta, L.D.L.T., Huang, J., et al. (2016). Genome-wide changes in lncRNA, splicing, and regional gene expression patterns in autism. Nature *540*, 423–427. https://doi.org/10.1038/nature20612.

Reemst, K., Noctor, S.C., Lucassen, P.J., and Hol, E.M. (2016). The indispensable roles of microglia and astrocytes during brain development. Front. Hum. Neurosci. *10*, 566. https://doi.org/10.3389/fnhum.2016.00566.

Rube, H.T., Lee, W., Hejna, M., Chen, H., Yasui, D.H., Hess, J.F., Lasalle, J.M., Song, J.S., and Gong, Q. (2016). Sequence features accurately predict genome-wide MeCP2 binding in vivo. Nat. Commun. *7*, 11025–11112. https://doi.org/10.1038/ncomms11025.

Russo, F.B., Freitas, B.C., Pignatari, G.C., Fernandes, I.R., Sebat, J., Muotri, A.R., and Beltrão-Braga, P.C.B. (2018). Modeling the Interplay Between Neurons and Astrocytes in Autism Using Human Induced Pluripotent Stem Cells. Biol. Psychiatr. *83*, 569–578. https://doi.org/10.1016/j.biopsych.2017.09.021.

RZ, C., S, A., M, T., and R, J. (2001). Deficiency of methyl-CpG binding protein-2 in CNS neurons results in a Rett-like phenotype in mice. Nat. Genet. *27*, 327–331. https://doi.org/10.1038/85906.

Salter, M.W., and Stevens, B. (2017). Microglia emerge as central players in brain disease. Nat. Med. *23*, 1018–1027. https://doi.org/10.1038/nm.4397.

Schafer, D.P., Heller, C.T., Gunner, G., Heller, M., Gordon, C., Hammond, T., Wolf, Y., Jung, S., and Stevens, B. (2016). Microglia contribute to circuit defects in Mecp2 null mice independent of microglia-specific loss of Mecp2 expression. Elife *5*, e15224. https://doi.org/10.7554/eLife.15224.

Schafer, D.P., and Stevens, B. (2015). Brains, Blood, and Guts: MeCP2 Regulates Microglia, Monocytes, and Peripheral Macrophages. Immunity *42*, 600–602. https://doi.org/10.1016/j.immuni.2015.04.002.

Sellgren, C.M., Gracias, J., Watmuff, B., Biag, J.D., Thanos, J.M., Whittredge, P.B., Fu, T., Worringer, K., Brown, H.E., Wang, J., et al. (2019). Increased synapse elimination by microglia in schizophrenia patient-derived models of synaptic pruning. Nat. Neurosci. *22*, 374–385. https://doi.org/10.1038/s41593-018-0334-7.

Sharma, P., Mesci, P., Carromeu, C., McClatchy, D.R., Schiapparelli, L., Yates, J.R., Muotri, A.R., and Cline, H.T. (2019). Exosomes regulate neurogenesis and circuit assembly. Proc. Natl. Acad. Sci. USA *116*, 16086–16094. https://doi.org/10.1073/pnas.1902513116.

Skene, P.J., Illingworth, R.S., Webb, S., Kerr, A.R.W., James, K.D., Turner, D.J., Andrews, R., and Bird, A.P. (2010). Neuronal MeCP2 Is Expressed at Near Histone-Octamer Levels and Globally Alters the Chromatin State. Mol. Cell *37*, 457–468. https://doi.org/10.1016/j.molcel.2010.01.030.

Stevens, B., Allen, N.J., Vazquez, L.E., Howell, G.R., Christopherson, K.S., Nouri, N., Micheva, K.D., Mehalow, A.K., Huberman, A.D., Stafford, B., et al. (2007). The Classical Complement Cascade Mediates CNS Synapse Elimination. Cell *131*, 1164–1178. https://doi.org/10.1016/j.cell.2007.10.036.

Suter, B., Treadwell-Deering, D., Zoghbi, H.Y., Glaze, D.G., and Neul, J.L. (2014). Brief report: MECP2 mutations in people without rett syndrome. J. Autism Dev. Disord. *44*, 703–711. https://doi.org/10.1007/s10803-013-1902-z.

Suzuki, M., Yamada, T., Kihara-Negishi, F., Sakurai, T., and Oikawa, T. (2003). Direct association between PU.1 and MeCP2 that recruits mSin3A-HDAC complex for PU.1-mediated transcriptional repression. Oncogene *22*, 8688–8698. https://doi.org/10.1038/sj.onc.1207182.

Tillotson, R., and Bird, A. (2020). The Molecular Basis of MeCP2 Function in the Brain. J. Mol. Biol. *432*, 1602–1623. https://doi.org/10.1016/j.jmb.2019.10.004.

Trujillo, C.A., Adams, J.W., Negraes, P.D., Carromeu, C., Tejwani, L., Acab, A., Tsuda, B., Thomas, C.A., Sodhi, N., Fichter, K.M., et al. (2021). Pharmacological reversal of synaptic and network pathology in human MECP2-KO neurons and cortical organoids. EMBO Mol. Med. *13*, e12523. https://doi.org/10.15252/EMMM.202012523.

Trujillo, C.A., Gao, R., Negraes, P.D., Chaim, I.A., Domissy, A., Vandenberghe, M., Devor, A., Yeo, G.W., Voytek, B., and Muotri, A.R. (2018). Nested oscillatory dynamics in cortical organoids model early human brain network development. Preprint at bioRxiv. https://doi.org/10.1101/358622.

Van den Veyver, I.B., and Zoghbi, H.Y. (2000). Methyl-CpG-binding protein 2 mutations in Rett syndrome. Curr. Opin. Genet. Dev. *10*, 275–279. http://www.ncbi.nlm.nih.gov/pubmed/10826991.

Vivanti, A.J., Vauloup-Fellous, C., Prevot, S., Zupan, V., Suffee, C., Cao, J.D., Benachi, A., and De Luca, D. (2020). Transplacental transmission of SARS-CoV-2 infection. Nat. Commun. *11*, 3572. https://doi.org/10.1038/s41467-020-17436-6.

Wang, J., Wegener, J.E., Huang, T.-W., Sripathy, S., De Jesus-Cortes, H., Xu, P., Tran, S., Knobbe, W., Leko, V., Britt, J., et al. (2015). Wild-type microglia do not reverse pathology in mouse models of Rett syndrome. Nature *521*, E1–E4. https://doi.org/10.1038/nature14444.

Ylisaukko-Oja, T., Rehnström, K., Vanhala, R., Kempas, E., Von Koskull, H., Tengström, C., Mustonen, A., Õunap, K., Lähdetie, J., and Järvelä, I. (2005). MECP2 mutation analysis in patients with mental retardation. Am. J. Med. Genet. *132A*, 121–124. https://doi.org/10.1002/ajmg.a.30416.

Zhang, Z.-N., Freitas, B.C., Qian, H., Lux, J., Acab, A., Trujillo, C.A., Herai, R.H., Nguyen Huu, V.A., Wen, J.H., Joshi-Barr, S., et al. (2016). Layered hydrogels accelerate iPSC-derived neuronal maturation and reveal migration defects caused by MeCP2 dysfunction. Proc. Natl. Acad. Sci. USA *113*, 3185–3190. https://doi.org/10.1073/pnas.1521255113.

Zhao, D., Mokhtari, R., Pedrosa, E., Birnbaum, R., Zheng, D., and Lachman, H.M. (2017). Transcriptome analysis of microglia in a mouse model of Rett syndrome: differential expression of genes associated with microglia/macrophage activation and cellular stress. Mol. Autism. *8*, 17. https://doi.org/10.1186/s13229-017-0134-z.

Zhu, Z., Mesci, P., Bernatchez, J.A., Gimple, R.C., Wang, X., Schafer, S.T., Wettersten, H.I., Beck, S., Clark, A.E., Wu, Q., et al. (2020). Zika Virus Targets Glioblastoma Stem Cells through a SOX2-Integrin αvβ5 Axis. Cell Stem Cell *26*, 187–204.e10. https://doi.org/10.1016/j.stem.2019.11.016.